Quantum detection of electronic flying qubits in the integer quantum Hall regime

G. Fève,[1,2] P. Degiovanni,[3,4] and Th. Jolicoeur[5]
[1]*Laboratoire Pierre Aigrain, Département de Physique de l'Ecole Normale Supérieure, 24 rue Lhomond, 75231 Paris Cedex 05, France*
[2]*Laboratoire de Photonique et Nanostructures, CNRS, Route de Nozay, 91460 Marcoussis, France*
[3]*Université de Lyon, Fédération de Physique André Marie Ampère, CNRS-Laboratoire de Physique de l'Ecole Normale Supérieure de Lyon, 46 Allée d'Italie, 69364 Lyon Cedex 07, France*
[4]*Department of Physics, Boston University, 590 Commonwealth Avenue, Boston, Massachusetts 02251, USA*
[5]*Laboratoire de Physique Théorique et Modèles Statistiques, Université Paris-Sud, 91405 Orsay Cedex, France*
(Received 1 August 2007; revised manuscript received 3 November 2007; published 8 January 2008)

We consider a model of a detector of ballistic electrons at the edge of a two-dimensional electron gas in the integer quantum Hall regime. The electron is detected by capacitive coupling to a gate which is also coupled to a passive *RC* circuit. Using a quantum description of this circuit, we determine the signal over noise ratio of the detector in terms of the detector characteristics. The backaction of the detector on the incident wave packet is then computed using a Feynman-Vernon influence functional approach. Using information theory, we define the appropriate notion of quantum limit for such an "on the fly" detector. We show that our particular detector can approach the quantum limit up to logarithms in the ratio of the measurement time over the *RC* relaxation time. We argue that such a weak logarithmic effect is of no practical significance. Finally, we show that a two-electron interference experiment can be used to probe the detector induced decoherence.

DOI: 10.1103/PhysRevB.77.035308 PACS number(s): 03.65.Yz, 03.65.Ta, 73.23.−b, 73.43.Cd

I. INTRODUCTION

Among qubit implementations, solid-state devices such as superconducting qubits[1] or quantum dot qubits based on charge[2] or spin degrees of freedom[3] are especially promising because of their potential scalability. Were decoherence problems solved, complex circuits involving several qubits, quantum gates, and detectors could, in principle, be manufactured using standard nanofabrication techniques. However, contrarily to recently proposed trapped ions[4] and Rydberg atom[5] architectures, solid-state qubits cannot be displaced at will. Thus, any quantum computing architecture based on solid-state qubits requires a quantum bus efficiently transmitting quantum information between various parts of the circuit.[6] An example of a quantum bus architecture is provided by circuit QED, in which superconducting qubits are coupled through one stationary mode of a superconducting resonator.[7] Experimental realization of circuit QED devices has been achieved recently.[8]

Another example involves flying qubits based on electrons propagating at the edge of a two-dimensional electron gas (2DEG) in the integer quantum Hall regime. These flying qubits have been proposed as the building block of a quantum computation architecture[9] or to perform quantum state transfer between charge or spin qubits.[10] In fact, in the presence of a quantizing magnetic field, edge modes are an almost ideal chiral ballistic system without any backscattering and with millimetric elastic mean free path. Recently, the on-demand injection of an energy resolved electronic edge excitation has been experimentally demonstrated.[11] Detection of single-electron edge excitations is the next crucial step needed to build quantum Hall flying qubit devices. Although detection of charge density waves at the edge of a quantum Hall droplet has already been demonstrated in an experiment by Ashoori *et al.*,[12] it is desirable to extend such measurements to the single-electron regime for quantum computation purposes.

In this paper, we present a model for the detection of single-electron edge excitations of a 2DEG in the integer quantum Hall effect (IQHE) regime. Our detector is based on a capacitive coupling between the 2DEG and a mesoscopic gate connected to a resistor modeling, for example, the input impedance of an ultralow noise cryogenic preamplifier. In this *RC* circuit, the capacitance corresponds to the capacitive coupling between the 2DEG and the metallic gate. The voltage across the resistance (i.e., before the amplification stage) is the detected signal unraveling the motion of a single-electron wave packet beneath the gate. The dissipative element (i.e., the resistor) is at finite temperature T.

An especially important quantity is the signal to noise ratio of the detector. We derive it by solving for the quantum dynamics of the circuit when a single-electron edge excitation goes through the gated region. As expected, a high impedance is needed to obtain a signal to noise ratio of order unity. On average, when the input impedance is close to the quantum of resistance $R_K=h/e^2$, about one microwave photon is emitted when a single-electron excitation moves through the gated region. Since performing quantum operations on flying qubits requires quantum coherence of the edge excitations, we have analyzed extensively the backaction of the detector on the electronic wave packet. The Feynman-Vernon influence functional[13] provides a very convenient tool to discuss damping, spreading, and spatial decoherence of the electronic wave packet induced by the detector. A complete solution is obtained in the case of chiral edge excitations with linear dispersion relation. In particular, analytic formulas are obtained in the low temperature regime, where noise in the resistor is expected to be minimum and dominated by quantum fluctuations. Contrarily to a continuous weak measurement in which the detector is constantly interacting with the qubit, the electronic flying qubit interacts

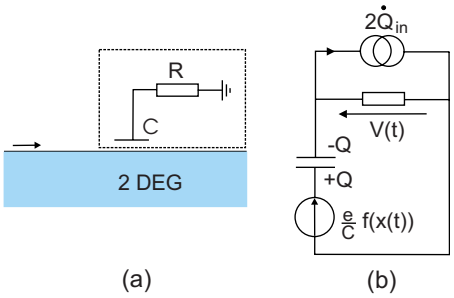

FIG. 1. (Color online) (a) The detector modeled as a resistor capacitively coupled to the edge of a 2DEG. (b) Equivalent circuit for the detector. The edge excitation in the 2DEG is seen as a transcient voltage source $(e/C)f(x(t))$ on the bottom part of the circuit. Noise in the resistor appears as the current generator on the top part of the circuit.

with our detector during its transit time through the gated region. Thus, the quantum limit cannot be defined in terms of the ratio of a measuring time to a decoherence time. As shown by Clerk *et al.*,[14] information theory provides an appropriate framework for defining the quantum limit. At very low temperatures, a similar analysis is developed here. An information theoretical measurement efficiency is defined and expressed in terms of the detector's parameters. It enables us to find optimal working parameters for the detector so that information taken away by the detector is most efficiently used in the detection process. For the present detector, the optimal measurement efficiency is obtained when the measurement time is not too large compared with the response time of the detector. A compromise on the detector's dissipation is needed to optimize the efficiency while keeping a reasonable signal to noise ratio.

In Sec. II, our model for the quantum Hall flying qubit detector is presented. The signal-associated with a single-electron edge excitation and the corresponding signal to noise ratio are computed in Sec. III. In Sec. IV, we discuss the backaction of the detector on a single-electron excitation using the Feynman-Vernon influence formalism. Then, the issue of decoherence is addressed in Sec. V. In Sec. VI, we suggest that a two-electron collision experiment can be used to probe the spatial decoherence induced by the detector. Consequences for experiments and conclusions are presented in Sec. VII.

II. MODELING THE DETECTOR

A. Presentation of the model

The detecting device consists of a gate capacitively coupled to the electronic states of a 2DEG. The typical gate length l is of the order of 10–100 μm, much larger than the Fermi wavelength. Any disturbance of the charge density of the 2DEG induces a voltage across the gate capacitance which is then amplified. In the present paper, the detector will be characterized by a resistive input impedance R at effective temperature T. The detection circuit will thus be modeled as an equivalent RC circuit (see Fig. 1), where C denotes the 2DEG/gate capacitance and R the input resistance. The detected signal is the voltage drop $V(t)$ across the resistance. Of course, this simplified model does not include a detailed description of the amplifier, but it already contains all the ingredients needed to discuss the physics of flying qubit detection and, in particular, the backaction of the detector on the qubit. Because we are studying the single charge detection problem, quantum fluctuations of the detector might play an important role. Therefore, the detection circuit shall be treated quantum mechanically.

The motion of the electrons in the two-dimensional gas is assumed to be ballistic and one dimensional. This assumption is satisfied in high mobility samples where the elastic mean free path may reach the millimeter range. In the IQHE regime at $\nu=1$, the low energy excitations of the 2DEG are edge excitations which can be described as chiral fermions with linear dispersion relation. For the sake of completeness and having in mind detection of charges within one-dimensional quantum wires, the case of nonrelativistic fermions with a quadratic dispersion relation will also be considered.

Since we are interested in single-electron wave packets localized over a distance Δx comparable to the gate size l, we will consider the detection of wave packets injected at energy ϵ_0 above the Fermi energy. The Heisenberg principle imposes $\epsilon_0 \gg \hbar v_F/l$, where v_F is the Fermi velocity within the considered energy range. Note that in a 2DEG, the Fermi velocity being of the order of 10^5 m s^{-1}, the typical temperature scale $\hbar v_F/k_B l$ is of the order of 100 mK for a 10 μm gate. In this regime, the electron is injected far above the Fermi level with respect to the energy scales associated with both the temperature and the detector. Therefore, filled energy levels can be neglected and the detection problem is reduced to the study of one excess charge coupled to the quantum RC circuit in a single-electron picture.

There are three relevant time scales in the system. The first one is the circuit response time equal to RC. For a high impedance detector ($R \sim 10^4$ Ω) and $C \sim 1$ fF μm^{-1}, it is of the order of 100 ps for a 10 μm gate and usually scales with l. Having a fast detector implies that this time scale is the smallest one in the problem. In particular, it has to be shorter than the traveling time $\mathcal{T}=l/v_F$ for the excitation below the gate. This sets the time resolution of the detector. For a 10–100 μm gate, $\mathcal{T}$ is of the order of 100 ps–1 ns and, thus, the fast detection criterion $RC \ll \mathcal{T}$ is realized for $R \leqslant 10^4$ Ω. Finally, the thermal time scale $\hbar/k_B T$ gives the memory time of voltage fluctuations within the RC circuit at temperature T. The $k_B T \ll \hbar v_F/l$ regime is called the low temperature regime, whereas $k_B T \gg \hbar v_F/l$ is called the high temperature regime of the detector.

B. Input/output formalism

To describe the quantum dynamics of the RC circuit, we follow the quantum network approach of Yurke and Denker[15] and model the dissipative element as a semi-infinite ($z \geqslant 0$) transmission line of characteristic impedance R. Such a transmission line is characterized by a continuous distribution of capacitance by unit length $\mathcal{C}_T$ and inductance $\mathcal{L}_T$ with specific choice $\sqrt{\mathcal{L}_T/\mathcal{C}_T}=R$. The transmission line is closed

by the discrete capacitance C at $z=0$. The distributed charge along the line is denoted by $Q(z,t)$ and describes the transmission line degrees of freedom. For $z>0$, it satisfies a one-dimensional wave equation:

$$\mathcal{L}_T \frac{\partial^2 Q}{\partial t^2} - \frac{1}{C_T}\frac{\partial^2 Q}{\partial z^2} = 0. \tag{1}$$

The solutions are forward and backward propagating waves with velocity $v=1/\sqrt{\mathcal{L}_T C_T}$:

$$Q(z,t) = Q_{in}\left(t+\frac{z}{v}\right) + Q_{out}\left(t-\frac{z}{v}\right), \tag{2}$$

whose Fourier decompositions can be written as

$$Q_{in}(t) = \sqrt{\frac{\hbar}{4\pi R}}\int_0^\infty \frac{d\omega}{\sqrt{\omega}}[a_{in}(\omega)e^{-i\omega t} + \text{H.c.}], \tag{3}$$

$$Q_{out}(t) = \sqrt{\frac{\hbar}{4\pi R}}\int_0^\infty \frac{d\omega}{\sqrt{\omega}}[a_{out}(\omega)e^{-i\omega t} + \text{H.c.}]. \tag{4}$$

The discrete capacitance C appears as a boundary condition on $z=0$ for the transmission line:

$$\frac{1}{C_T}\frac{\partial Q}{\partial z}(0,t) - \frac{Q(0,t)}{C} = 0. \tag{5}$$

Using the notation $Q(t)$ for the charge of the capacitor at the end of the line $Q(t)=Q(z=0,t)$, the boundary condition can be rewritten as

$$R\dot{Q}(t) + \frac{Q(t)}{C} = 2R\dot{Q}_{in}(t). \tag{6}$$

An electron propagating in the 2DEG underneath the gate induces a charge q_{ind} on the gate. In a single particle approach, it can be written as $q_{ind}(t)=ef(x(t))$, where $x(t)$ is the position of the electron with respect to the gate at time t. The function f accounts for the shape of the gate. A realistic device will have a typical gate size of the order of 10 μm to be compared to a spacing of 100 nm between the 2DEG and the gate. Thus, the 2DEG-gate coupling in the neighborhood of $x=0$ will be close to unity: almost all the electric field lines will go from the passing electron to the gate. Thus, we will only consider the simplified case of optimal coupling $f(x=0)=1$ (we note that the less than optimal situation leads to similar results). Far away from the detector, $f(x\to\pm\infty)=0$ as the electron does not feel the presence of the gate. The typical width of the function $f(x)$ is the size of the gate l, much greater than the Fermi wavelength. In full generality, $f(x)=h(2x/l)$, where $h(u)$ decays rapidly for $|u|\leqslant 1$. In this paper, a triangular shape function will often be used to obtain explicit results. It is defined by $f(x)=0$ for $|x|\geqslant l/2$ and $f(x)=1-2|x|/l$ for $|x|\leqslant l/2$. Although the shape function f is not universal, this specific case will enable us to get explicit analytical results which capture the essential physics of the problem.

The induced charge appears as a source term added to the noise term in Eq. (6):

$$R\dot{Q}(t) + \frac{Q(t)}{C} = 2R\dot{Q}_{in}(t) + \frac{e}{C}f(x(t)). \tag{7}$$

The equations of motion (1) and (7) can be derived from a Lagrangian of the form

$$L = L_{el} + L_0 + L_\partial, \tag{8}$$

where L_{el} is the Lagrangian of the electronic system and L_0 is the bulk Lagrangian for the transmission line:

$$L_0 = \int_0^{+\infty}\left[\frac{\mathcal{L}_T}{2}\left(\frac{\partial Q}{\partial t}\right)^2 - \frac{1}{2C_T}\left(\frac{\partial Q}{\partial z}\right)^2\right]dz. \tag{9}$$

The boundary Lagrangian L_∂ corresponds to the electrostatic energy stored in the capacitance, and describes the interaction between the charge $Q(0,t)$ and the induced charge:

$$L_\partial = -\frac{1}{2C}[Q(0,t) - ef(x(t))]^2. \tag{10}$$

The RC circuit degrees of freedom are the modes propagating along the transmission line. They are easily quantized by imposing the usual commutation relations for the bosonic modes:

$$[a_\alpha(\omega), a_\beta^+(\omega')] = \delta(\omega-\omega')\delta_{\alpha,\beta}, \tag{11}$$

where α and β stand for *in* and *out* operators. The Lagrangian (8) will be used within a path integral formalism when discussing decoherence of the electronic wave packet.

In this paper, two possible forms for the electronic Lagrangian L_{el} will be considered: (i) the case of a chiral electron with relativistic (linear) dispersion appropriate for describing the edge excitations of a $\nu=1$ droplet and (ii) the case of a nonrelativistic particle with parabolic dispersion. The latter will allow a more complete understanding of the specifics of chiral edge excitations.

III. EVOLUTION OF THE CIRCUIT

In this section, the evolution of the detector during the measurement process is discussed. As a first step, we shall consider a classical charge moving along a fixed trajectory in the 2DEG. The signal generated by such a moving charge will be computed and expressed in terms of the number of microwave photons sent into the detector. This signal will be compared to the input noise generated by the preamplifier. We will provide explicit expressions for the corresponding signal to noise ratio.

A. Detected signal

1. Quantum signal in the input/output formalism

Let us compute the circuit's evolution when a charge e travels in the 2DEG along a given trajectory $t\mapsto x(t)$. Solving for the time evolution equation (7) gives access to the voltage drop in the transmission line $V(t)=-(1/C_T)\partial Q/\partial z = [ef(t)-Q(t)]/C$. This voltage is the input signal for the preamplifier and is equal to

$$V(t) = -\frac{1}{C}\sqrt{\frac{\hbar}{\pi R}}\int_0^\infty \frac{\sqrt{\omega}}{\omega - 1/iRC} a_{in}(\omega)e^{-i\omega t} + \text{H.c.}$$
$$+ \frac{e}{RC^2}\int_0^\infty d\tau e^{-\tau/RC}[f(t) - f(t-\tau)], \quad (12)$$

where $f(t)$ stands for $f(x(t))$. The first term corresponds to the quantum noise generated by the resistor, and the second term is the signal created by the external charge. The average voltage is obtained by tracing over the transmission line degrees of freedom. Only the second term of Eq. (12) contributes to the average voltage:

$$\langle V(t)\rangle = \frac{e}{RC^2}\int_0^\infty d\tau e^{-\tau/RC}[f(t) - f(t-\tau)]. \quad (13)$$

A good detector is expected to react faster than the characteristic time $\mathcal{T}=l/v_F$ of the electron-gate interaction. Assuming that the electron velocity is very close to the Fermi velocity v_F, the fast detector condition is $RC \ll \mathcal{T}$. For a fast detector, the average detected voltage becomes $\langle V(t)\rangle = Re\frac{df}{dt}$.

2. Photon emission

A rough estimate for photon emission into the detection circuit can be obtained noticing that the typical voltage generated by a single charge is $eR/\mathcal{T}$. This electromagnetic pulse lasts for time $\mathcal{T}$. Thus, the total energy emitted is of the order $R^{-1}(eR/\mathcal{T})^2\mathcal{T} \sim e^2R/\mathcal{T}$. Assuming photons have a frequency $\mathcal{T}^{-1}$, the typical number of photons emitted into the detector during the measurement is $\bar{n}_m \sim e^2R/\hbar = 2\pi R/R_K$, where $R_K = h/e^2$ is the resistance quantum. A first implication of this result is the need for a high impedance detector in order to limit the total acquisition time.

Let us denote by $\mathcal{E}(\omega)$ the spectral density of the energy dissipated in the resistor during measurement of a single charge traveling at fixed velocity v_F. It is given in terms of the Fourier transform $\tilde{V}(\omega)$ of the average voltage $\langle V(t)\rangle$ by $\mathcal{E}(\omega) = |\tilde{V}(\omega)|^2/2\pi R$. Then, Eq. (13) leads to

$$\mathcal{E}(\omega) = \hbar\frac{R}{R_K}\frac{\omega^2}{\omega^2 + \frac{1}{(RC)^2}}\left(\frac{l}{2v_FRC}\right)^2\left|\tilde{h}\left(\frac{\omega l}{2v_F}\right)\right|^2, \quad (14)$$

where the gate shape function f is written as $f(x) = h(2x/l)$, and $\tilde{h}$ denotes the Fourier transform of h. This expression shows that the RC circuit acts as a high pass filter cutting frequencies below $1/RC$. The shape of the gate acts as a low pass filter. For a fast detector, the latter dominates and photon emission preferably takes place around frequency v_F/l.

B. Signal to noise ratio

1. General expressions

The signal to noise ratio is an important characteristic of a detector. In the present case, a first estimate can already be obtained using the above photon number estimations. In the low temperature limit $k_BT \ll \hbar v_F/l$, most of the modes where photon emission takes place are unpopulated. Therefore, we expect $\bar{n}_m$ to provide a crude estimate for the signal to noise ratio of the measurement device, which would then be of the order of R/R_K. In the high temperature regime $k_BT \gg \hbar v_F/l$, all the relevant modes will be populated by $lk_BT/\hbar v_F$ photons corresponding to the thermal noise of the detector. Therefore, the signal to noise ratio should be reduced by this factor in the high temperature regime. This discussion also shows that the low temperature regime is also a quantum regime with respect to the modes relevant for detection.

Let us now turn toward a more precise definition of the signal to noise ratio. Let us consider as our signal the voltage collected over $\mathcal{T}/2$:

$$\bar{V}(t) = \frac{2}{\mathcal{T}}\int_t^{t+\mathcal{T}/2} d\tau V(\tau). \quad (15)$$

Contrarily to the voltage collected over a time $\mathcal{T}$, this quantity does not vanish on average. Assuming a triangular gate function of width l and a fast detector, the maximum average signal when the electron passes through the gate is given by

$$\langle\bar{V}\rangle = \frac{2Re}{\mathcal{T}}\int_0^{\mathcal{T}/2} d\tau\frac{df}{d\tau} = \frac{2Re}{\mathcal{T}}, \quad (16)$$

where bracketing $\langle . \rangle$ denotes quantum statistical averaging at temperature T. The fluctuation $\Delta\bar{V}^2 = \langle\bar{V}^2\rangle - \langle\bar{V}\rangle^2$ is directly related to the symmetrized noise correlator $g(\tau) = \langle\{V_I(\tau), V_I(0)\}_+\rangle/2$, where V_I denotes the voltage operator in the interaction representation. Explicitly, it is given by

$$g(\tau) = \frac{\hbar}{\pi RC^2}\int_0^\infty \coth\left(\frac{\hbar\omega}{2k_BT}\right)\frac{\omega\cos(\omega\tau)}{\omega^2 + \left(\frac{1}{RC}\right)^2}d\omega, \quad (17)$$

which, for a triangular gate of width l, leads to

$$\Delta\bar{V}^2 = \frac{\hbar}{\pi RC^2}\int_0^\infty \coth\left(\frac{\hbar\omega}{2k_BT}\right)\frac{\sin^2\left(\frac{\omega\mathcal{T}}{4}\right)}{\left(\frac{\omega\mathcal{T}}{4}\right)^2}\frac{\omega d\omega}{\omega^2 + \left(\frac{1}{RC}\right)^2}. \quad (18)$$

Finally, the signal to noise ratio (SNR) is defined as

$$\text{SNR}_T = \frac{\langle\bar{V}\rangle^2}{\langle\bar{V}^2\rangle - \langle\bar{V}\rangle^2}. \quad (19)$$

2. Asymptotics and numerical results

At vanishing temperatures and for a fast detector, the signal to noise ratio saturates to a value given by

$$\text{SNR}_0 \simeq \frac{R}{R_K}\frac{\pi^2}{\log\left[\frac{l}{2v_FRC}\right] + \gamma}, \quad (20)$$

where γ is the Euler constant $\gamma \approx 0.577$. The logarithmic correction with respect to $2\pi R/R_K$ shows that the signal to

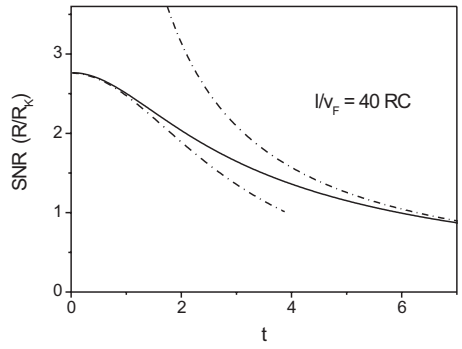

FIG. 2. The signal to noise ratio divided by R/R_K as a function of the dimensionless temperature $tk_BT/(\hbar v_F/l)$ and for $l/v_F=40\,RC$ (full lines). Dashed dotted lines represent the high and low temperature asymptotics, respectively, given by Eq. (22) and Eqs. (20) and (21).

noise ratio is optimized by decreasing the measurement time within the limits of fast measurement.

As expected and as shown in Fig. 2, the signal to noise ratio decreases with increasing temperature. In the very low temperature regime $k_BT \ll \hbar v_F/l \ll \hbar/RC$, the temperature dependence can be extracted by noticing that, in the noise integral (18), $\coth(\hbar\omega/2k_BT)-1$ departs from zero in a frequency range much lower than v_F/l and $1/RC$. We obtain

$$\frac{1}{\mathrm{SNR}_T}-\frac{1}{\mathrm{SNR}_0}=\frac{R_K}{24R}\left(\frac{k_BT}{\hbar v_F/l}\right)^2. \tag{21}$$

In the high temperature limit $k_BT \gg \hbar v_F/l$, we have

$$\mathrm{SNR}_T \simeq 2\pi\frac{R}{R_K}\frac{\hbar v_F/l}{k_BT}. \tag{22}$$

Having characterized the evolution of the detection circuit as well as its signal to noise ratio, we will now turn to its backaction on the electronic degrees of freedom.

IV. EVOLUTION OF THE ELECTRONIC DEGREES OF FREEDOM

In this section, the quantum backaction of the detector on the edge excitations will be analyzed. Within a path integral formalism, the Feynman-Vernon approach[13] gives access to the electronic evolution by integrating out the *RC* circuit degrees of freedom through the so-called influence functional. This functional contains all information on dissipation (energy relaxation) and decoherence caused by the interaction with the detector. After a brief reminder of the Feynman-Vernon formalism, the nonrelativistic (quadratic dispersion relation) and chiral fermion (linear dispersion relation) cases will be successively considered.

A. General formalism

The Feynman-Vernon formalism is based on an explicit integration over the environmental degrees of freedom treated as an effective bath of harmonic oscillators in thermal equilibrium. Let us denote the initial electronic reduced density operator by $\rho_{0,el}$, and $\rho_{0,r}$ the one associated with the detector. Then, at time $t \geqslant 0$, the electron reduced density operator is given by

$$\rho_{el}(x_f^+,x_f^-,t)=\langle x_f^+|\mathrm{Tr}_r(U(t)(\rho_{0,el}\otimes\rho_{0,r})U^+(t))|x_f^-\rangle. \tag{23}$$

Note that, here, a factorized initial condition is appropriate since the electron injection is performed on demand at a given time.[11] In full generality, this reduced density operator will evolve according to

$$\rho_{el}(x_f^+,x_f^-,t)=\int J_t\begin{pmatrix}x_f^+ & x_i^+\\ x_f^- & x_i^-\end{pmatrix}\rho_{0,el}(x_i^+,x_i^-)dx_i^+dx_i^-. \tag{24}$$

The evolution kernel can be expressed within a path integral formalism in terms of the action for a free electron moving in the classical potential created by the gate $S_{el}=\int[L_{el}-e^2f(x)^2/2C]d\tau$ and in terms of the Feynman-Vernon (FV) influence functional $\exp(-\Phi_{FV}[x^+,x^-])$ representing the backaction of the detector:

$$J_t\begin{pmatrix}x_f^+ & x_i^+\\ x_f^- & x_i^-\end{pmatrix}=\int \mathcal{D}[x^+,x^-]e^{i/\hbar S_{el}[x^+,x^-]}e^{-\Phi_{FV}[x^+,x^-]}, \tag{25}$$

where $S_{el}[x^+,x^-]=S_{el}[x^+]-S_{el}[x^-]$. In this equation, the boundary conditions are given by $x^\pm(t)=x_f^\pm$ and $x^\pm(0)=x_i^\pm$. Considering the resistor to be in equilibrium with temperature T, the Feynman-Vernon influence functional $\exp(-\Phi_{FV}[x^+,x^-])$ is Gaussian:

$$\Phi_{FV}[x^+,x^-]=\frac{e^2}{\hbar RC^2}\int_0^t d\tau\int_0^\tau du[f[x^+(\tau)]-f[x^-(\tau)]]\times[L(\tau-u)f[x^+(u)]-\bar{L}(\tau-u)f[x^-(u)]], \tag{26}$$

$$L(\tau-u)=\int_0^\infty\frac{d\omega}{\pi}\frac{\omega}{\omega^2+(1/RC)^2}\left\{\coth\left(\frac{\hbar\omega}{2k_BT}\right)\cos[\omega(\tau-u)]-i\sin[\omega(\tau-u)]\right\}. \tag{27}$$

The real part of Φ_{FV} is responsible for decoherence, and the imaginary part describes dissipation. The $\coth\left(\frac{\hbar\omega}{2k_BT}\right)$ factor that relates them is a direct consequence of the detailed balance condition expressing that the gate is initially at equilibrium with temperature T. Note that the free evolution action $S_{el}[x^+,x^-]$ depends on whether chiral fermions in the quantum Hall regime or nonrelativistic fermions with quadratic dispersion relation are considered.

B. Quadratic dispersion relation

We will now study the usual case of free fermions with a quadratic dispersion relation $\epsilon_k=\hbar^2k^2/2m$, where m is the electron effective mass. In the high temperature regime $k_BT \gg \hbar v_F/l$, the problem is greatly simplified since the Feynman-Vernon influence functional becomes local in time. The spreading of the electronic wave packet and the energy damping caused by the gate can be calculated in a semiclassical approach.

As shown in Appendix A, the probability distribution for the particle is then described by a Langevin equation that can be directly derived from the Feynman-Vernon formalism:

$$m\ddot{r} + e^2 R f'(r)^2 \dot{r} = f'(r)\xi(t), \tag{28}$$

where $\xi(t)$ denotes a classical Gaussian noise:

$$\langle \xi(t_1)\xi(t_2)\rangle = 2Re^2 k_B T \delta(t_1 - t_2). \tag{29}$$

1. Energy relaxation

Equation (28) shows that interaction with the gate also introduces a position dependent friction force proportional to the electronic velocity. This friction force leads to the energy relaxation for the particle. Assuming weak dissipation, the velocity will remain close to v_F and, thus, approximating $f'(r) \approx f'(v_F t)$ leads to an exponential damping of the velocity:

$$\langle v(t)\rangle = v_F \exp\left[-\frac{e^2 R}{m} \int_0^t d\tau f'(v_F \tau)^2 \right]. \tag{30}$$

In the case of a triangular gate of width l, the above expression gives the velocity drop after the particle has crossed the gate:

$$\frac{\langle v_{\text{after}}\rangle}{\langle v_{\text{before}}\rangle} = \exp\left(-4 \frac{R}{R_K} \frac{\lambda_F}{l} \right), \tag{31}$$

where $\lambda_F = \hbar / m v_F$ denotes the Fermi wavelength (typically $\lambda_F \sim 20$ nm in AsGa). Since $l \gg \lambda_F$, the weak dissipation assumption is satisfied for $R \lesssim R_K$.

2. Spreading of the wave packet

Let us now focus on the evolution of the width $\delta r^2 = \langle (r - \langle r\rangle)^2\rangle$ of the electronic wave packet due to the gate. Neglecting the electronic velocity damping, the spreading of the wave packet $\Delta_{\delta r^2}(t) = \delta r^2(t) - \delta r^2(0)$ is given by

$$\Delta_{\delta r^2}(t) = \frac{4Re^2 k_B T}{m^2} \int_0^t d\tau_1 \int_0^{\tau_1} d\tau_2 \int_0^{\tau_2} d\tau_3 f'(v_F \tau_3)^2. \tag{32}$$

In the case of a triangular gate, the total spreading $\Delta_{\delta r^2}$ due to the interaction with the gate is given by

$$\Delta_{\delta r^2} = \frac{8}{3} \frac{R}{R_K} \frac{k_B T}{h v_F / l} \lambda_F^2. \tag{33}$$

Scaling like λ_F^2, the wave packet spreading is expected to be small although it might be observable for high enough temperature.

The full evolution of the electron reduced density matrix can be described in the high temperature regime using a Markovian master equation. Contrarily to the usual quantum Brownian motion, decoherence and friction terms depend on the gate shape function f, making an exact solution impossible. An approximate solution to this equation describing decoherence induced by the gate at high temperatures is given in Appendix C. However, it is not valid in the low temperature regime potentially relevant for future experiments. As we shall see now, in the case of chiral fermions with linear dispersion relation, an exact solution can easily be obtained, leading to a fully general expression for the spatial decoherence induced by the measurement.

C. Chiral fermions

1. Exact real time evolution

Let us now consider chiral fermions with linear dispersion. In this case, the static potential $e^2 f(x)^2 / 2C$ created by the gate does not lead to any backscattering, but only to an additional forward scattering phase with respect to the free chiral fermion evolution:

$$U_0(t)|x\rangle = \exp\left[-\frac{ie^2}{2\hbar C v_F} \int_x^{x+v_F t} du f(u)^2 \right] |x + v_F t\rangle. \tag{34}$$

Therefore, the position operator evolves according to the free ballistic evolution for chiral fermions propagating at the Fermi velocity v_F: $x(t) = x(0) + v_F t$. Because of this very simple evolution of the position operator, the right-hand side (rhs) of Eq. (23) can be evaluated by going to the interaction scheme with respect to the gate-electron interaction. Introducing $x_i^{\pm} = x_f^{\pm} - v_F t$, we have

$$\rho_{el}(x_f^+, x_f^-, t) = \rho_{0,el}(x_i^+, x_i^-) e^{i(\phi_+ - \phi_-)} \mathcal{D}_t(x_f^+, x_f^-), \tag{35}$$

where the phase $e^{i(\phi_+ - \phi_-)}$ is given by $\phi_{\pm} = \frac{e^2}{2\hbar C} \int_0^t f(x_f^{\pm} - v_F \tau)^2 d\tau$ and corresponds to the forward scattering phase induced by the gate. Because of chirality and linear dispersion for the edge excitations, dissipation only introduces a multiplicative decoherence factor $\mathcal{D}_t(x_f^+, x_f^-)$ given by

$$\mathcal{D}_t(x_f^+, x_f^-) = \mathrm{Tr}_r(U_I[x_f^+, t] \rho_{0,r} U_I^{\dagger}[x_f^-, t]), \tag{36}$$

where $U_I[x,t] = T \exp\left[-i \frac{e}{\hbar C} \int_0^t f(x - v_F(t - \tau)) Q_I(\tau) d\tau \right]$. Equation (36) shows that this decoherence coefficient is simply given by the Feynman-Vernon influence functional evaluated for the classical trajectories $x_{\pm}(\tau) = x_i^{\pm} + v_F \tau$. Therefore, we have

$$\mathcal{D}_t(x_f^+, x_f^-) = e^{-\Phi_{FV}[x_f^+, x_f^-]}, \tag{37}$$

where

$$\Phi_{FV}[x_f^+, x_f^-] = \frac{e^2}{\hbar R C^2} \int_0^t d\tau \int_0^{\tau} d\tau' [f[x_f^+, \tau] - f[x_f^-, \tau]] \times [L(\tau - \tau') f[x_f^+, \tau'] - \bar{L}(\tau - \tau') f[x_f^-, \tau']], \tag{38}$$

$$f[x, \tau] = f[x - v_F(t - \tau)]. \tag{39}$$

Equations (35) and (37)–(39) provide the complete solution for the dynamics of a chiral edge excitation with exact linear dispersion in the presence of the detector modeled as an RC circuit. Remember that our "on the fly" detector influences the chiral edge excitation only while traveling near the gate. Because of this finite interaction time, $x_f^{\pm}$ are chosen on the

right side of the gate, corresponding to positions after interaction with the detector. Accordingly, the time scale t is chosen so that $x_i^{\pm}=x_f^{\pm}-v_F t$ is on the left side of the gate. This is equivalent to extending integration limits in Eq. (38) to the half-plane $\tau' \leqslant \tau$.

2. Dissipation

Before considering how the detector affects the spatial quantum coherence of the chiral fermion, it is important to discuss energy dissipation associated with the detection process. As explained in Sec. II A, the effect of the Fermi sea has been neglected because the extra charge has been injected high enough above the Fermi level. It is thus important to check that this assumption remains valid through the detection process. The discussions of Sec. III A 2 and IV B 1 already show that this is indeed the case. Focusing on the low temperature regime which gives the best signal to noise ratio and assuming $R \lesssim R_K$, the typical energy emitted is of the order of $(R/R_K)\times(\hbar v_F/l) \lesssim \hbar v_F/l$. This corresponds to the energy loss of the detected electron and, therefore, since $\epsilon_0 \gg \hbar v_F/l$, the detection process does not bring it back to the Fermi level.

Finally, the coupling to the gate leads to a destruction of spatial coherence existing prior to the interaction with the gate. A detailed study of the spatial decoherence induced by the gate is presented in Sec. V and its consequences on a two-electron collision experiment are presented in Sec. VI.

V. DECOHERENCE OF THE ELECTRONIC WAVE PACKET

A. General discussion

In this section, we will focus on the decay of spatial coherence for the chiral edge excitation. It is directly related to the real part of the Feynman-Vernon exponent $\Phi_{FV}(x_f^+,x_f^-)$:

$$\left|\frac{\rho_{el}(x_f^+,x_f^-,t)}{\rho_{0,el}(x_i^+,x_i^-)}\right| = e^{-\mathrm{Re}[\Phi_{FV}(x_f^+,x_f^-)]}. \tag{40}$$

Since the coupling to the detector takes place during a short window of time corresponding to the passing time l/v_F of edge excitations beneath the gate, Eq. (40) will be used to evaluate the decay of spatial coherence after the whole detection process. This is achieved by taking a wide enough range of integration in the explicit expression for $\Phi_{FV}(x_f^+,x_f^-)$ given by Eqs. (38) and (39). The resulting decoherence exponent $\Gamma_c(d)=\mathrm{Re}(\Phi_{FV}(x_f^+,x_f^-))$ then only depends on the distance $d=|x_f^+-x_f^-|$ over which spatial coherence is probed and on the detector's parameters (size l, response time RC, and temperature T). Its general expression is

$$\Gamma_c(d) = \frac{e^2}{\hbar RC^2}\int_{0\leqslant\tau'\leqslant\tau} \Delta_f(\tau)\mathrm{Re}[L(\tau-\tau')]\Delta_f(\tau')d\tau d\tau', \tag{41}$$

where $\Delta_f(\tau)=f[x_f^+,\tau]-f[x_f^-,\tau]$. In the large separation limit $d\to\infty$, only diagonal contributions associated with products $f[x,\tau]f[x,\tau']$ survive and give the residual coherence:

$$\Gamma_c(\infty) = \frac{2e^2}{\hbar RC^2}\int_{\tau'\leqslant\tau} f[x,\tau]\mathrm{Re}[L(\tau-u)]f[x,\tau']d\tau d\tau' \tag{42}$$

which is indeed independent of x. Note that this contribution only probes the noise kernel of the detector over the detection time scale l/v_F. When d decreases, the off-diagonal contribution involving products $f[x_f^{\pm},\tau]f[x_f^{\mp},\tau]$ in Eq. (41) become important. It is sensitive to the noise over a time scale d/v_F. Assuming that the noise evaluated at $|\tau-\tau'|=d/v_F$ varies smoothly over l/v_F, an estimate for the off diagonal contribution is then

$$\Gamma_c^{(\mathrm{od})}(d) \simeq -\frac{\pi\eta}{2}\frac{R}{R_K}\left(\frac{l}{RCv_F}\right)^2 \mathrm{Re}\left[L\left(\frac{d}{v_F}\right)\right], \tag{43}$$

where $\eta=[\int h(u)du]^2$ accounts for the precise shape of the gate. Assuming the RC circuit has memory time τ_m, saturation of decoherence will be actually reached for $d \gtrsim v_F\tau_m$.

For small separation $d \ll l$, the decoherence exponent is expected to scale as $(d/l)^2$. The exact expression can be derived by expanding $\Delta(\tau)=\frac{d}{v_F}\frac{\partial f}{\partial\tau}[\bar{x}_f]$, where $x_f^{\pm}=\bar{x}_f\pm d/2$:

$$\Gamma_c(d) = \frac{e^2d^2}{\hbar RC^2v_F^2}\int_{\tau'\leqslant\tau} d\tau d\tau' \frac{df}{d\tau}[\bar{x}_f,\tau]\mathrm{Re}[L(\tau-\tau')]\frac{df}{du}[\bar{x}_f,\tau']. \tag{44}$$

The decoherence exponent will now be evaluated and discussed in the various temperature regimes of the detector. Asymptotic expressions will be derived in the case of $d \to \infty$ and $d \ll l$, and compared to numerical evaluations of $\Gamma_c(d)$ for the case of a triangular gate.

B. Results for a triangular gate

In the case of a triangular gate, an integral expression valid in all regimes is easily obtained:

$$\Gamma_c(d) = 16\frac{R}{R_K}\int_0^{+\infty} \frac{\sin^4(\lambda_l x)\sin^2(2\lambda_d x)}{\lambda_l^2 x^4}\frac{x\coth(\alpha x)}{x^2+1}dx, \tag{45}$$

where $\lambda_l=l/4v_FRC$ and $\alpha=\hbar(RC)^{-1}/2k_BT$. This expression is plotted on Fig. 3 as a function of d/l for various temperatures.

1. Zero temperature limit

For small separation $d \ll l$, we have

$$\Gamma_c(d) \simeq 24\left[\log\left(\frac{l}{2v_FRC}\right)+\gamma-\frac{\log(2)}{3}\right]\frac{R}{R_K}\left(\frac{d}{l}\right)^2. \tag{46}$$

For large separation $d \gg l$, the decoherence exponent saturates at

$$\Gamma_c(\infty) = 8\log(2)\frac{R}{R_K}. \tag{47}$$

As mentioned above, the memory time of the RC circuit is responsible for the large d/l behavior of the decoherence

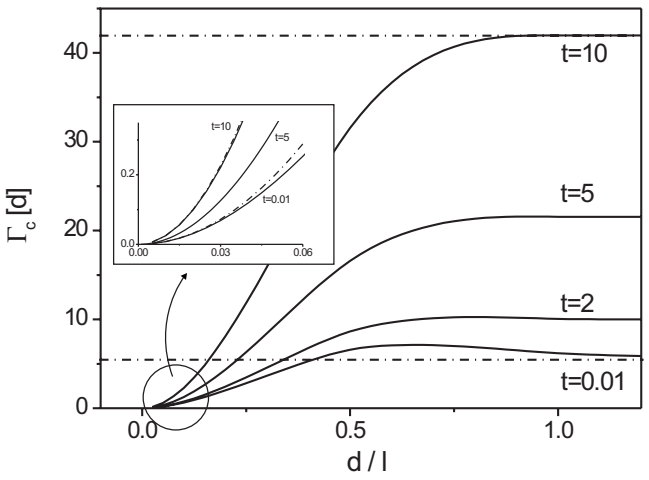

FIG. 3. Decoherence exponent $\Gamma_c(d)$ as a function of d/l for various dimensionless temperatures $t=k_BT/(\hbar v_F/l)$ for $l/v_F=40$ *RC* (full line). The inset shows the behavior at short distance with typical $(d/l)^2$ behavior. Dotted lines show the $d \ll l$ and $d \gg l$ asymptotics given by Eqs. (46) and (47) for very low temperature and by Eqs. (51) and (52).

coefficient [see Eq. (43)]. At low temperature, the noise kernel of the *RC* circuit behaves as $(-1/\pi)[RC/(\tau-\tau')]^2$ and, therefore, this shows that decreasing d leads to an increase of the decoherence exponent:

$$\Gamma_c^{(\mathrm{od})}(d) \simeq \frac{\eta}{2}\frac{R}{R_K}\left(\frac{l}{d}\right)^2. \tag{48}$$

Equivalently, it means that decreasing d from a very large value first leads to a stronger decoherence. This result is a direct consequence of the long range correlations present in the *RC* circuit at very low temperatures. This effect is expected to be weak $(l/d \ll 1)$ and disappears rapidly with increasing temperature.

2. High temperature limit

In the high temperature limit, the noise kernel can be considered as local in time $\mathrm{Re}[L(s)] \simeq 2(RC)^2(k_BT/\hbar)\delta(s)$ and, therefore, the decoherence exponent is explicitly given by

$$\Gamma_c(d) = 2\pi\frac{R}{R_K}\frac{k_BT}{\hbar v_F/l}\int \Delta(y,d/l)^2\frac{dy}{l}, \tag{49}$$

$$\Delta(y,d/l) = h\left(y+\frac{d}{l}\right) - h\left(y-\frac{d}{l}\right). \tag{50}$$

Note that the coefficient in front of geometrical factor $\int \Delta(y,d/l)^2 dy/l$ scales as the thermal photon number $\frac{k_BT}{\hbar v_F/l}$, reflecting the increase of fluctuations with temperature. As expected, the decoherence exponent saturates at $d \to \infty$ and also scales as $(d/l)^2$ for $d \ll l$. In the case of a triangular gate function, these expressions can be explicitly evaluated in the small $d \ll l$ and large distance $d \gg l$ limits:

$$\Gamma_c(d \to 0) \simeq 8\pi\frac{R}{R_K}\frac{k_BT}{\hbar v_F/l}\left(\frac{d}{l}\right)^2, \tag{51}$$

$$\Gamma_c(\infty) = \frac{4\pi}{3}\frac{R}{R_K}\frac{k_BT}{\hbar v_F/l}. \tag{52}$$

C. Efficiency and quantum limit for flying qubit detection

We are now in a position to characterize the efficiency of the flying qubit detection. However, in the present detection scheme, the electronic edge excitation and the detector interact during a finite time l/v_F. Therefore, the notion of quantum limit cannot be defined by referring to the measurement and dephasing rates which do not make sense here. Indeed, as stressed in the Introduction, it should be approached through the basic concepts of information theory. Clerk *et al.* have shown that the quantum limit can be understood from an information theory perspective:[14] the quantum limit is reached when the information extracted by the detector is entirely used for the measurement.

We will now elaborate on this general idea having in mind the optimization of flying qubit detection. For simplicity, the discussion will focus on the case of chiral edge excitations with linear dispersion relation. We will first discuss the accessible information stored in the detector while probing two edge excitations initially located at two different positions. Then, the ability of the measurement scheme to distinguish between the two initial positions using the voltage signal (12) will be discussed quantitatively using information theory. The detector efficiency will then be defined in terms of these two notions and will be used to discuss its optimization as well as its ability to reach the quantum limit.

1. Accessible information

Let us consider the interaction between a coherent wave packet described by the wave function ψ_0 at time $t_i=0$ and the detector. At zero temperature, the electron+detector state at time t is precisely of the form generalizing Eq. (14) of Ref. 14:

$$\int \psi_0(x)|x+v_Ft\rangle \otimes |D_t(x)\rangle dx, \tag{53}$$

where

$$|D_t(x)\rangle = T\exp\left[-\frac{i}{\hbar}\int_0^t f(x+v_F\tau)Q_I(\tau)d\tau\right]|0\rangle. \tag{54}$$

As seen above, since $f(x+v_F\tau)=0$ at large enough times, the t dependence can safely be dropped out. Each state $|D(x)\rangle$ is a tensor product of coherent states over all the modes propagating in the transmission line $|D(x)\rangle \otimes_\omega |\alpha_\omega(x)\rangle$. The information relative to the position x of the edge excitation is stored in the phases of the complex amplitudes characterizing these coherent states.

Different initial positions x^+ and x^- of the edge excitation correspond to different phases, and this leads to the measure-

ment induced decoherence $e^{-\Gamma_c(d)}=|\langle D(x^-)|D(x^+)\rangle|$, where $d=|x^+-x^-|$. This decoherence coefficient is indeed an infinite product of contributions corresponding to all the propagating modes of the transmission line:

$$e^{-\Gamma_c(d)}=\left|\prod_{\omega=0}^{\infty}\langle\alpha_\omega(x^-)|\alpha_\omega(x^+)\rangle\right|. \quad (55)$$

Therefore, introducing the spectral density $\Gamma_c(d,\omega)$ of the decoherence exponent $\Gamma_c(d)$, the contribution of scalar products associated with modes within $[\omega,\omega+d\omega]$ in the rhs of Eq. (55) is equal to

$$\prod_{\omega\leqslant\omega'\leqslant\omega+d\omega}^{\infty}|\langle\alpha_{\omega'}(x^-)|\alpha_\omega(x^+)\rangle|\sim 1-\Gamma_c(d,\omega)d\omega. \quad (56)$$

Therefore, summing Eq. (24) of Clerk *et al.*[14] over all the modes, the quantum mechanical accessible information associated with the pair of states $|D(x^+)\rangle$ and $|D(x^-)\rangle$ is given by

$$\mathcal{I}[x^+,x^-]=\int_0^\infty\Gamma_c(d,\omega)d\omega=\Gamma_c(d). \quad (57)$$

This equation shows that the decoherence exponent has a direct information-theoretic interpretation.

2. Measurement information

Let us now provide an estimate for the information associated with the measurement process. For the sake of simplicity, we will restrict ourselves to the problem of distinguishing between two initial positions x^+ and x^- separated by a distance d. These corresponds to the two possible inputs of the communication channel associated with the complete detection device.

Detection of an edge excitation is performed through the classical signal average over a time $\mathcal{T}/2$ [see Eq. (15)]. In the case of a fast detector $RC\ll\mathcal{T}$, the signal created by an edge excitation initially located at x is given by

$$\bar{V}(t)=\frac{2eRv_F}{l}\left[f\left(x+\frac{l}{2}+v_Ft\right)-f(x+v_Ft)\right]. \quad (58)$$

Let us now consider two average signals $\bar{V}_\pm(t)$ associated with initial positions $x^\pm$ separated by a distance d. The difference between these two signals can be used to distinguish between x^+ and x^-. It clearly follows from Eq. (58) that the maximum difference at a given time t varies from $(4Rev_F/l)\times(d/l)\times\max(|h'(u+l/2)-h'(u)|)$ for $d\ll l$ to $4Rev_F/l$ for $d=l/2$, and then decreases to $2eRv_F/l$ when $d\gg l$.

Because of the noise within the detector, the signal at time t is distributed according to a Gaussian whose variance is given by Eq. (18). Therefore, the mutual information associated with two signals having $|\bar{V}_+-\bar{V}_-|=\max_t(|\bar{V}_+(t)-\bar{V}_-(t)|)$ and variance $\Delta\bar{V}$ can be expressed as

$$R(\lambda)=\log(2)-\frac{\lambda}{2}\int_0^\infty e^{-(\lambda z)^2/8}F(\lambda,z)\frac{dz}{\sqrt{2\pi}}, \quad (59)$$

$$F(\lambda,z)=\log((1+e^{-(\lambda^2/2)(z+1)})(1+e^{(\lambda^2/2)(z-1)})), \quad (60)$$

where $\lambda=|\bar{V}_+-\bar{V}_-|/\Delta\bar{V}$. In general, λ depends on d, the details of the gate shape function, and the signal to noise ratio computed in Sec. III B. The measurement information $\Gamma_m(d)=R(\lambda(d))$ represents the maximum rate of information collected through the detector if one modulates the edge excitation sources by sending trains of either delayed or advanced localized electrons separated by a time d/v_F.

For $d\ll l$, up to some coefficient that reflects the details of the gate shape function, $\lambda\simeq 4\sqrt{\mathrm{SNR}_0}\times(d/l)$. In the opposite limit $d\gg l$, $\lambda\sim\sqrt{\mathrm{SNR}_0}$. The behavior of $R(\lambda)$ in various limits is also very simple. For $\lambda\to\infty$, $R(\lambda)\to\log(2)$. It reflects the fact that the measurement delivers exactly one bit of information since it enables to distinguish unambiguously between x^+ and x^-. In the $\lambda\ll 1$ limit, $R(\lambda)\simeq\lambda^2/8$, which leads to a $(d/l)^2$ scaling for $d\ll l$: the detector hardly distinguishes two very close initial positions.

3. Measurement efficiency and optimization

Knowing the accessible information $\Gamma_c(d)$ and the measurement information $\Gamma_m(d)$, we define the measurement efficiency as $\Gamma_m(d)/\Gamma_c(d)$.

At short distances ($d\ll l/\sqrt{\mathrm{SNR}_0}$), we have

$$\Gamma_m(d)\sim 2\mathrm{SNR}_0\times(d/l)^2 \quad (61)$$

and, therefore, the efficiency of the measurement becomes independent of R/R_K and only depends on the size of the gate since $\Gamma_c(d)$ scales as $(R/R_K)(d/l)^2$. Using expression (20) for the zero temperature signal to noise ratio, this leads to

$$\frac{\Gamma_m(d)}{\Gamma_c(d)}\simeq\frac{\pi^2/12}{\left[\gamma-\frac{\log(2)}{3}+\log\left(\frac{l}{2v_FRC}\right)\right]\left[\gamma+\log\left(\frac{l}{2v_FRC}\right)\right]}. \quad (62)$$

Optimizing the detector requires the choice of a low value for l/v_FRC and, in this case, this also corresponds to the optimization of the signal to noise ratio for a fixed R/R_K.

Contrarily to the short distance case, the efficiency at large distances ($d\gg l$) depends on R/R_K. At very large R/R_K, the signal to noise ratio increases indefinitely, but this does not improve the measurement information. The high decoherence then leads to a low efficiency that goes as $R_K/8R$. More generally, we have shown that $\mathrm{SNR}_0=(R/R_K)\times\kappa_{\mathrm{SNR}}(l/v_FRC)$, where κ_{SNR} depends on the shape of the gate. In the same way, for $d\to\infty$, Eq. (42) tells us that at zero temperature, $\Gamma_c(\infty)=(R/R_K)\times\kappa_c(l/v_FRC)$. Thus, the measurement efficiency at large distances is given by

$$\frac{\Gamma_m(\infty)}{\Gamma_c(\infty)}=\frac{\kappa_{\mathrm{snr}}}{8\kappa_c}\times\frac{8R(\sqrt{\mathrm{SNR}_0})}{\mathrm{SNR}_0}. \quad (63)$$

Remarkably, the ratio of Eq. (63) to its very weak coupling value is a universal function of the signal to noise ratio:

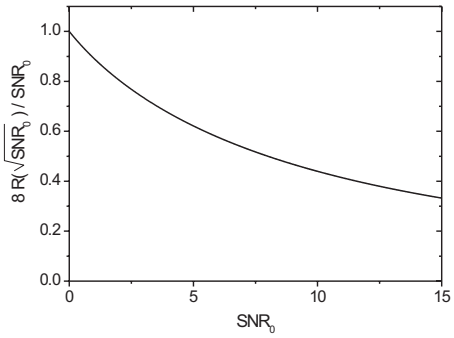

FIG. 4. Ratio of the large distance ($d \to \infty$) efficiency for arbitrary coupling R/R_K to its value in the very weak coupling limit ($R/R_K \ll 1$).

$$\frac{(\Gamma_m/\Gamma_c)(\infty)}{\lim_{R/R_K \to 0}((\Gamma_m/\Gamma_c)(\infty))} = \frac{8R(\sqrt{\mathrm{SNR}_0})}{\mathrm{SNR}_0}. \tag{64}$$

This function is plotted in Fig. 4. It suggests that a reasonable signal to noise ratio $\mathrm{SNR}_0 \sim 1$ can be reached without losing too much in terms of efficiency compared to the weak coupling situation. In the limit of a weakly coupled detector ($R \ll R_K$), the efficiency tends to $\kappa_{\mathrm{SNR}}/8\kappa_c$, which depends on the gate shape. It is generically a decreasing function of $l/2v_F RC$. As in the short distance case, decreasing $l/v_F RC$ at fixed R/R_K corresponds to optimizing the mode structure in order to minimize decoherence while ensuring an efficient measurement.

Figure 5 shows the inverse of the efficiency computed for $d=l/2$ as a function of $l/2v_F RC$ for a triangular gate, taking into account the exact formula (13) integrated over time $\mathcal{T}/2$ so that the finite response time of the circuit is taken into account.

These curves exhibit a rather weak dependence in $l/2v_F RC$ even down to values where the fast detector approximation is not expected to work. They also show that going from a weakly coupled detector $R/R_K \lesssim 0.1$ to a high impedance one $R/R_K \sim 1$ for $l/2v_F RC \sim 5$ leads to a drop of the efficiency by 50%, while increasing the signal to noise ratio by a factor 10. Typical values range from 0.2 to 0.1,

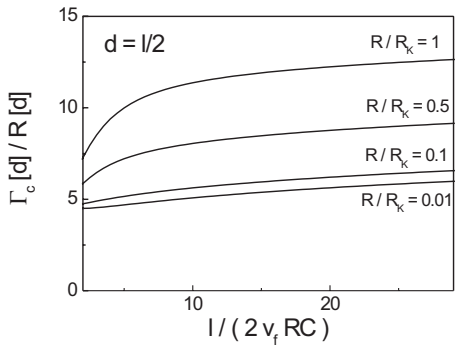

FIG. 5. Inverse of the efficiency as a function of $l/2v_F RC$ for various values of R/R_K. These curves are computed for a triangular gate taking into account the finiteness of RC and not making the fast detector approximation.

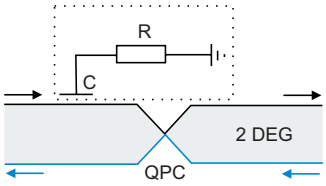

FIG. 6. (Color online) Principle scheme for a two-electron collision experiment within a 2DEG. Electronic edge excitations are injected into the incoming edge channels (incoming arrows) and detected on the outgoing channels (outcoming arrows) after having passed through the QPC. A detector (dotted box) is located on one of the incoming edge channels.

which shows that the quantum RC circuit does not reach the quantum limit in the sense of $\Gamma_m(l/2)/\Gamma_c(l/2) \sim 1$. A slower detector would reach an efficiency of 0.25 in the weak coupling regime and 0.15 at $R/R_K = 1$.

VI. EFFECT OF DECOHERENCE ON A TWO-ELECTRON COLLISION

We now describe an experiment which enables detecting decoherence of the electronic wave packet by the detector. The idea is to perform a two-electron collision through a quantum point contact that acts as a beam splitter for the electronic edge excitations. In the case of bosons, photons bunch together and tend to come out through the same quantum channel. Only recently has bunching of photons emitted by independent sources been experimentally demonstrated by Beugnon *et al.*[16] Here, because of the Pauli principle, antibunching is expected: the electrons should leave into different outgoing channels after passing through the beam splitter. On the other hand, classical particles should partition randomly, thus leading to a probability of 1/4 for leaving both in a given outgoing channel, and 1/2 for leaving in different channels. As we shall see, introducing the flying qubit detector on one of the input channels leads to an intermediate behavior interpolating between full antibunching and the partition behavior depending on the decoherence introduced by the detector. We consider only the case of complete spin polarization as appropriate for a 2DEG in the IQHE regime. The realization of an electronic Mach-Zehnder interferometer operating precisely in these conditions has recently been performed.[17]

The geometry of the experiment is described in Fig. 6: two edge states labeled by + and −, corresponding to the different directions of propagation (tracks) on the opposite sides of the sample, are connected through a quantum point contact (QPC) located at $x=0$. Such a quantum point contact tuned at transmission 1/2 realizes the analog of an optical beam splitter. Denoting the state corresponding to the position x on track $\pm$ by $|x, \pm\rangle$, the QPC action on one-particle states is given by

$$|x_i, +\rangle \to \frac{1}{\sqrt{2}}(|x_f, +\rangle + |x_f, -\rangle), \tag{65}$$

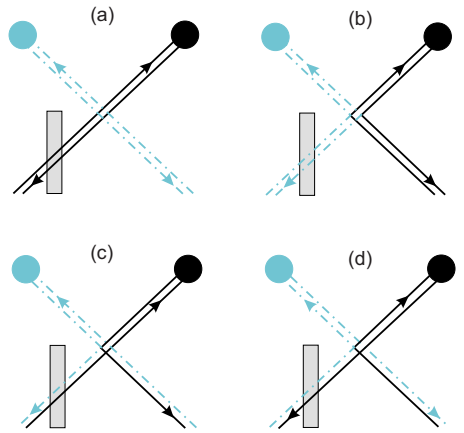

FIG. 7. (Color online) Space-time diagrams for the probability P_{+-}: the vertical axis represents time, whereas the horizontal one represents space. The blue and black dots represent destructive detection on the + and − output edge channels of the device. Trajectories connected to the dots have the same color (blue ones are also dashed-dotted for convenience). Upward arrows indicate forward branches in the Feynman-Vernon double path integral, whereas downward arrows indicate backward branches. A straight trajectory means that the particle remains on the same track, whereas a broken trajectory involves a jump from one track to the other at the QPC. The gray rectangle represents the action of our detector. Diagrams (a) and (b) correspond to the classical partition by the QPC, whereas diagrams (c) and (d) contain exchange effects associated with identical quantum particles.

$$|x_i,-\rangle \to \frac{1}{\sqrt{2}}(|x_f,+\rangle - |x_f,-\rangle), \tag{66}$$

assuming that x_i is located before the QPC with respect to electron propagation, and $x_f=x_i+v_F t$ is located after it. The flying qubit detector is located on one of the input channels which are fed with the same wave function $\psi(x+x_0)$ centered around a position $x_i=-x_0$, where

$$\psi(x) = \left(\frac{2}{\pi a^2}\right)^{1/4} e^{ik_F x} e^{-x^2/a^2}. \tag{67}$$

Antibunching of the particles is probed through the probabilities of joint detection after collision on the beam splitter on the same outgoing edge channel (say, +) P_{++} or on opposite edge channels P_{+-}. The probability P_{++} can be computed as the probability to find both electrons on edge state + at position $x_f-\delta/2 \leqslant x \leqslant x_f+\delta/2$, where x_f is the central position of the detecting area and $\delta \gg a$ so that this detecting area fully overlaps the electronic wave packets. For the probability P_{+-}, indiscernability of the particles is taken into account by symmetrizing the projection operator under the exchange of both particles.

For classical distinguishable particles, the probability P_{+-} is the sum of two contributions: one in which particles remain on the same track and one in which particles change track while crossing the QPC. These correspond to space-time diagrams (a) and (b) in Fig. 7. They involve decoherence coefficients along parallel trajectories that reach the same detection point of space time. Thus, along these trajectories, the distance $|(x^+-x^-)(\tau)|$ remains small (exactly zero for chiral fermions). Therefore, these contributions are unaffected by the presence of the detector.

For quantum identical particles, quantum statistics enters the game. The initial quantum state is a symmetrized or antisymmetrized two-particle state depending on the bosonic or fermionic character of the particles. Therefore, the probability P_{+-} also contains quantum contributions that are represented by diagrams (c) and (d) in Fig. 7. In these contributions, the decoherence coefficient involves trajectories that are not connected to the same terminal detection points in space-time. Therefore, these contributions are much more sensitive to the effect of the gate since they feel the difference in the positions of the detection points. In the limit of very strong decoherence, the decoherence factor that weight contributions (c) and (d) kills them, giving back the results that would be obtained for distinguishable particles.

Assuming that the two particles were initially injected with the same wave function on the two input branches, the probabilities P_{+-} and P_{++} in the presence of the gate are equal to

$$P_{+-} = \frac{1}{4}\int |\psi(x)\psi(x')|^2(1+e^{-\mathrm{Re}[\Phi_{FV}(x,x')]})dxdx', \tag{68}$$

$$P_{++} = \frac{1}{4}\int |\psi(x)\psi(x')|^2(1-e^{-\mathrm{Re}[\Phi_{FV}(x,x')]})dxdx'. \tag{69}$$

Thus, the two-particle interference can potentially probe the decoherence coefficient associated with the gate. Recent experiments have been able to observe electronic interference in an electronic Mach-Zehnder setup and coherence lengths of order 20 μm have been reported.[18,19] Visibility of fringes up to 90% have been obtained.[20] The same device has also detected the signature of two-particle interferences on current cross correlations, thus demonstrating quantum coherence along a path length of 2×8 μm. This suggests that the manipulations envisioned in this paper could be performed in the near future.

VII. CONCLUSION AND PERSPECTIVES

We have performed a detailed analysis of a solid-state device appropriate for the detection of flying qubits at the edge of a two-dimensional electron gas in the IQHE regime. A very special feature of this device is that the interaction with the electron is restricted to a small interval of time. As a consequence, it is no longer possible to discuss the quantum limit of measurement by comparison of a measurement time and a decoherence time. However, we have shown that, by invoking information-theoretic concepts, the appropriate notion of quantum limit can be defined. Using this approach, we have discussed in a very explicit way the deviation from the quantum limit as well as the detector optimization, having in mind the perspective of forthcoming experiments.

Although the present work focuses on a very simple detector scheme, our approach could, in principle, be used to deal with more realistic situations. A detection scheme based

on a damped oscillator treated as an *LC* circuit connected to a transmission line[21] could be treated using our method. However, one could also think of using a mesoscopic detector such as a nanotube transistor[23] or a quantum point contact, the latter being known for its ability to reach the quantum limit in a continuous measurement.[14,22] A more realistic description of the preamplifier in the quantum regime is needed. Its backaction could be accounted for within the present formalism assuming it generates a Gaussian noise, possibly out of equilibrium. Note that taking more precisely the added noise and the associated quantum constraints into account would lead to a precise description of the output amplified signal. Recently, measurement of the state of a qubit using a Josephson bifurcation amplifier has been performed.[24] In this dispersive measurement technique, the backaction noise arises from sources that can be thermalized efficiently to the lowest temperature available. Inventing and studying a nonlinear bifurcation amplifier able to work in the presence of a high magnetic field would certainly be an interesting perspective for flying qubit detection.

ACKNOWLEDGMENTS

We thank the Mesoscopic Physics group at LPA-ENS for constant interaction during this work. P.D. acknowledges support from the Condensed Matter Theory visitors program at Boston University.

APPENDIX A: DERIVATION OF THE LANGEVIN EQUATION

The idea is to compute the effective action to the leading order in the quantum fluctuation $\Delta(t)=x^+(t)-x^-(t)$ and to derive a semiclassical equation of motion for the average position variable $r(t)=\frac{1}{2}(x^+(t)+x^-(t))$. In the high temperature regime, the effective action for the electron becomes local:

$$\frac{iS}{\hbar}=i\frac{m}{\hbar}\int dt\dot{r}\dot{\Delta}-i\frac{e^2R}{\hbar}\int dtf'(r)^2\dot{r}\Delta - \frac{e^2Rk_BT}{\hbar^2}\int dtf'(r)^2\Delta^2. \tag{A1}$$

Considering the kernel (24) for $x_f^+=x_f^-=x_f$ and $x_i^+=x_i^-=x_i$, integrating the first part and transforming the last Gaussian term into a Gaussian integral over the auxiliary field ξ leads to the following path integral:

$$J_t\begin{pmatrix}x_f & x_i\\ x_f & x_i\end{pmatrix}=\int \mathcal{D}[r,\Delta,\xi]\exp\left[-\int d\tau\frac{\xi(\tau)^2}{4e^2Rk_BT}\right]\times\exp\left\{i\hbar^{-1}\int d\tau\Delta(\tau)[-m\ddot{r}(\tau) - e^2Rf'(r(\tau))^2\dot{r}(\tau) + f'(r(\tau))\xi(\tau)]\right\} \tag{A2a}$$

$$=\int \mathcal{D}[r,\xi]\exp\left[-\int d\tau\frac{\xi(\tau)^2}{4e^2Rk_BT}\right]\times\prod_{\tau=0}^{t}\delta[m\ddot{r}(\tau)+e^2Rf'(r(\tau))^2\dot{r}(\tau) - f'(r(\tau))\xi(\tau)], \tag{A2b}$$

where $r(0)=x_i$ and $r(t)=x_f$. The second line follows from the first by integration over the quantum fluctuation Δ. The rhs of Eq. (A2b) describes the Langevin equation (28) and its associated noise (29).

APPENDIX B: THE DECOHERENCE FACTOR FOR CHIRAL FERMIONS

In full generality, the Feynman-Vernon influence functional for a pair of trajectories $[x^+(\tau),x^-(\tau)]$ is defined by tracing out over the *RC* circuit degrees of freedom. In operatorial form, it is given by

$$\mathcal{F}[x^+,x^-]=\mathrm{Tr}(U_I[x^+,t]\,.\,\rho_{r,0}\,.\,U_I^\dagger[x^-,t]), \tag{B1}$$

where $U_I[x^\pm,t]$ denotes the evolution operator between $t_i=0$ and t for the *RC* circuit in the presence of an electron moving along $x^\pm(\tau)$:

$$U_I[x^\pm,t]=T\exp\left[-i\frac{e}{\hbar C}\int_0^t f(x^\pm(\tau))Q_I(\tau)d\tau\right]. \tag{B2}$$

In the case of chiral fermions, the electron dynamics can be solved exactly in the interaction representation, leading to Eq. (35). Using Eq. (B1), the decoherence coefficient given by Eq. (36) is precisely equal to the Feynman-Vernon influence functional for trajectories $x^\pm(\tau)=x_i^\pm+v_F\tau$. In the case considered here, the Feynman-Vernon influence functional is a Gaussian functional of $\tau\mapsto f(x^\pm(\tau))$ given by Eqs. (26) and (27).

APPENDIX C: MASTER EQUATION FOR DECOHERENCE

In the high temperature limit, the evolution of the density matrix can be rewritten as a master equation:

$$\frac{\partial\rho_{el}(t)}{\partial t}=\frac{i\hbar}{2m}\left[\frac{\partial^2}{\partial x^2}-\frac{\partial^2}{\partial x'^2}\right]\rho_{el} \tag{C1a}$$

$$-\frac{e^2R}{2m}[f(x)-f(x')]\times\left[f'(x)\frac{\partial}{\partial x}-f'(x')\frac{\partial}{\partial x'}\right]\rho_{el} \tag{C1b}$$

$$-\frac{e^2Rk_BT}{\hbar^2}[f(x)-f(x')]^2\rho_{el}. \tag{C1c}$$

Assuming the energy released by the edge is weak, we shall neglect the friction term (C1b) and focus on the decoherence term (C1c). The resulting simplified equation is rewritten as

$$\frac{\partial \rho_{el}(t)}{\partial t} = \frac{i\hbar}{2m}\left(\frac{\partial^2}{\partial x^2} - \frac{\partial^2}{\partial x'^2}\right)\rho_{el}(t) - \frac{e^2 R k_B T}{\hbar^2}[f(x) - f(x')]^2 \rho_{el}(t). \tag{C2}$$

We will look for a solution of Eq. (C2) in the following form:

$$\rho_{el}(t) = \rho_{\text{free}}(t) \times (\delta\rho)(t), \tag{C3}$$

where $\rho_{\text{free}}(t)$ describes the free evolution of the particles:

$$\langle x|\rho_{\text{free}}(t)|x'\rangle \sim e^{ik_F(x-x')} \exp\left[-\frac{(x - v_F t)^2}{a^2 + 2i\hbar t/m}\right] \times \exp\left[-\frac{(x' - v_F t)^2}{a^2 + 2i\hbar t/m}\right]. \tag{C4}$$

The evolution equation of $\delta\rho$ contains terms of the same form as the rhs of Eq. (C2) plus a contribution arising from single derivatives of $\rho_{\text{free}}(x,x',t)$ with respect to x and x'. Assuming that the smallest length scale in the problem is $\lambda_F = 2\pi/k_F$, the derivatives of $\rho_{\text{free}}(x,x',t)$ can be approximated by

$$\frac{\partial \rho_{\text{free}}}{\partial x} \simeq ik_F \rho_{\text{free}}(x,x',t), \tag{C5}$$

$$\frac{\partial \rho_{\text{free}}}{\partial x'} \simeq -ik_F \rho_{\text{free}}(x,x',t). \tag{C6}$$

The resulting contribution then dominates the kinetic energy term in the evolution equation for $\delta\rho$. With these approximations, the evolution of $\delta\rho$ is then given by

$$\frac{\partial(\delta\rho)}{\partial t} = -v_F\left(\frac{\partial}{\partial x} + \frac{\partial}{\partial x'}\right)(\delta\rho) - \frac{e^2 R k_B T}{\hbar^2}[f(x) - f(x')]^2(\delta\rho), \tag{C7}$$

whose solution is given by

$$(\delta\rho)(x_f^+, x_f^-, t) = \exp\left\{-\frac{e^2 R k_B T}{\hbar^2}\int_0^t [\Delta_f(\tau)]^2 d\tau\right\}, \tag{C8}$$

where $x_i^{\pm} = x_f^{\pm} - v_F t$ and $\Delta_f(\tau) = f(x_f^+ - v_F\tau) - f(x_f^- - v_F\tau)$. The effect of the interaction with the gate on the off-diagonal elements of the density matrix is the same as the one found in the high temperature limit for chiral fermions [see Eqs. (49) and (50)]. Indeed, Eq. (C7) is identical to the one expected for a linear dispersion relation $\epsilon_k = \hbar v_F k$. Keeping the leading terms of order k_F, we have neglected the small fluctuations of the velocity $\delta k \ll k_F$ around its mean value and we have taken $k \approx k_F$. This approximation is valid if the width of the wave packet δx is much larger than the Fermi wavelength λ_F, which means that we have a well defined excitation above the Fermi energy: $\delta\epsilon \ll \epsilon_f$.

[1] Yu. Makhlin, G. Schön, and A. Schnirman, Rev. Mod. Phys. **73**, 357 (2001).
[2] X. Hu and S. Das Sarma, Phys. Rev. A **61**, 062301 (2000).
[3] D. Loss and D. P. DiVincenzo, Phys. Rev. A **57**, 120 (1998).
[4] D. Kielpinski, C. Monroe, and D. J. Wineland, Nature (London) **417**, 709 (2002).
[5] J. Mozley, P. Hyafil, G. Nogues, M. Brune, J.-M. Raimond, and S. Haroche, Eur. Phys. J. D **35**, 43 (2005).
[6] D. P. DiVincenzo, Fortschr. Phys. **48**, 771 (2000).
[7] A. Blais, R. S. Huang, A. Wallraff, S. M. Girvin, and R. J. Schoelkopf, Phys. Rev. A **69**, 062320 (2004).
[8] A. Wallraff, D. I. Schuster, A. Blais, L. Frunzio, R. S. Huang, J. Majer, S. Kumar, S. M. Girvin, and R. J. Schoelkopf, Nature (London) **431**, 162 (2004).
[9] R. Ionicioiu, G. Amaratunga, and F. Udra, Int. J. Mod. Phys. B **15**, 125 (2001).
[10] T. M. Stace, C. H. W. Barnes, and G. J. Milburn, Phys. Rev. Lett. **93**, 126804 (2004).
[11] G. Fève, A. Mahé, J. M. Berroir, T. Kontos, B. Plaçais, D. C. Glattli, A. Cavanna, B. Etienne, and Y. Jin, Science **316**, 1169 (2007).
[12] R. C. Ashoori, H. L. Stormer, L. N. Pfeiffer, K. W. Baldwin, and K. West, Phys. Rev. B **45**, 3894 (1992).
[13] R. P. Feynman and F. L. Vernon, Ann. Phys. (N.Y.) **24**, 118 (1963).
[14] A. A. Clerk, S. M. Girvin, and A. D. Stone, Phys. Rev. B **67**, 165324 (2003).
[15] B. Yurke and J. S. Denker, Phys. Rev. A **29**, 1419 (1984).
[16] J. Beugnon, M. P. A. Jones, J. Dingjan, B. Darquié, G. Messin, A. Browaeys, and P. Grangier, Nature (London) **440**, 779 (2006).
[17] I. Neder, M. Heiblum, D. Mahalu, and V. Umansky, Phys. Rev. Lett. **98**, 036803 (2007).
[18] P. Roulleau, F. Portier, D. C. Glattli, P. Roche, A. Cavanna, G. Faini, U. Gennser, and D. Mailly, arXiv:0710.2806 (unpublished).
[19] G. Seelig and M. Büttiker, Phys. Rev. B **64**, 245313 (2001).
[20] I. Neder, N. Ofek, Y. Chung, M. Heiblum, D. Mahalu, and V. Umansky, Nature (London) **448**, 333 (2007).
[21] G. Johansson, L. Tornberg, and C. M. Wilson, Phys. Rev. B **74**, 100504(R) (2006).
[22] A. A. Clerk, Phys. Rev. Lett. **96**, 056801 (2006).
[23] A. Javey, J. Guo, D. B. Farmer, Q. Wang, E. Yenilmez, R. G. Gordon, M. Lundstrom, and H. J. Dai, Nano Lett. **4**, 1319 (2004).
[24] I. Siddiqi, R. Vijay, F. Pierre, C. M. Wilson, M. Metcalfe, C. Rigetti, L. Frunzio, and M. H. Devoret, Phys. Rev. Lett. **93**, 207002 (2004).